PRIMARY CENTERS AND SECONDARY CONCENTRATIONS OF TECTONIC ACTIVITY THROUGH TIME IN THE WESTERN HEMISPHERE OF MARS

Robert C. Anderson*
Jet Propulsion Laboratory
California Institute of Technology
Pasadena, CA 91109

James M. Dohm
Department of Hydrology and Water Resources
University of Arizona
Tucson AZ 85721

Matthew P. Golombek, Albert F.C. Haldemann, Brenda J. Franklin
Jet Propulsion Laboratory
California Institute of Technology
Pasadena, CA 91109

Kenneth L. Tanaka, Juan Lias
U.S. Geological Survey
Flagstaff AZ, 86001

Brian Peer
Dept. of Geology and Planetary Sciences
University of Pittsburgh
Pittsburgh, PA 15260

Submitted to the Journal of Geophysical Research
April 20, 2000

---

* Corresponding author, email: Robert.Anderson@jpl.nasa.gov.

Abstract

Five main stages of radial and concentric structures formed around Tharsis from the Noachian through the Amazonian as determined by geologic mapping of structures within the stratigraphic framework of Mars and by testing their orientations for radial and concentric orientations. Tectonic activity peaked in the Noachian (Stage 1) around the largest center, Claritas, a large, elongate rise, extending more than 20° in latitude defined by 8972 grabens that are concentrated in the Syria Planum, Thaumasia, and Tempe Terra regions. During the Late Noachian and Early Hesperian (Stage 2), extensional structures formed along the length of present day Valles Marineris and in Thaumasia (with a secondary concentration near Warrego Vallis) radial to a region just to the south of the central margin of Valles Marineris. Early Hesperian (Stage 3) radial grabens in Pavonis, Syria, Ulysses, and Tempe Terra and somewhat concentric wrinkle ridges in Lunae and Solis Plana and in Thaumasia, Sirenum, Memnonia, and Amazonis are centered northwest of Syria with secondary centers located at Thaumasia, Tempe Terra, Ulysses Fossae, and western Valles Marineris. Late Hesperian/Early Amazonian (Stage 4) structures around Alba Patera, the northeast-trending alignment of Tharsis Montes, and Olympus Mons appears centered on Alba Patera. Stage 5 structures (Middle-Late Amazonian) represent the last pulse of Tharsis-related activity and are found around the large shield volcanoes and are centered near Pavonis Mons. Tectonic activity around Tharsis began in the Noachian and generally decreased through geologic time to the Amazonian. Statistically significant radial distributions of structures formed during each stage, centered at different locations within the higher elevations of Tharsis. Secondary centers of radial structures during many of the stages appear related to previously identified local magmatic centers that formed at different times and locations throughout Tharsis.

Introduction

The western hemisphere of Mars is dominated by the formation of Tharsis, which is an enormous high-standing region (roughly 25% of the surface area of the planet) capped by a volcanic province containing the solar system's largest shield volcanoes. Tharsis is surrounded by an enormous radiating system of grabens and a sweeping circumferential system of wrinkle ridges that extends over the entire western hemisphere of Mars (Figure 1) [*Carr*, 1974; *Wise et al.*, 1979, *Plescia and Saunders*, 1982, *Scott and Dohm*, 1989, *Tanaka et al.*, 1991, *Banerdt et al.*, 1992]. This region is perhaps the largest single tectonic and volcanic province on the terrestrial planets with a rich and well preserved history of geologic and tectonic activity that has lasted throughout Martian geologic time. Unraveling the geologic and tectonic history of this region is critical to understanding the tectonic and geologic evolution of Mars.

Although quite a large number of studies have been completed on various aspects of the geologic and tectonic history of Tharsis, this is the first study to place all common structures within the western hemisphere of Mars into the global stratigraphic framework and the only study to use a comprehensive data set of all these structures to quantitatively evaluate their radial geometry as a clue to the causative stress field. Specifically, many studies have established the overall tectonic and geologic history of the Tharsis province [e.g., *Carr*, 1974; *Wise et al.*, 1979, *Plescia and Saunders*, 1982, *Scott and Dohm*, 1989, *Tanaka et al.*, 1991, *Banerdt et al.*, 1992] and many studies have developed detailed tectonic and geologic histories of local areas [e.g., *Frey*, 1979, *Tanaka and Davis*, 1988, *Tanaka*, 1990, *Scott and Dohm*, 1990b, *Dohm and Tanaka*, 1999], but no study has systematically placed all common structures into the global stratigraphic framework. In this study, we analyze the largest, most comprehensive paleotectonic dataset ever assembled; over 24,000 tectonic features in the western hemisphere of Mars were mapped,

classified, digitized and dated within the established stratigraphic framework of Mars [*Tanaka,* 1986]. This work has established the tectonic development of the entire western hemisphere of Mars, including the Tharsis province, and revealed the pattern of tectonic activity through time.

For the Tharsis region, grabens and wrinkle ridges form a system that appears radial and concentric; many workers have attempted to use the location and orientation of tectonic features around Tharsis to constrain the geometry of the causative stress field [e.g., *Wise et al.,* 1979, *Plescia and Saunders,* 1982, *Watters and Maxwell,* 1986, *Watters,* 1993, *Anderson,* 1988, *Golombek,* 1989]. However, these studies were restricted in unraveling the complete tectonic history of Tharsis because they used smaller structural datasets, concentrated on specific types of structures, and/or did not separate the different types of tectonic structures. In this study, we developed a comprehensive data set of common structures on Mars to quantitatively evaluate their true radial nature. Note that because the orientation of the structures is a result of the geometry of the stress field, traces of grabens and normals to wrinkle ridges can be used to test the radial nature of the causative stress fields and to see if different tectonic features and episodes had geometrically similar stress fields.

Methodology

The tectonic history of Mars is recorded in the distribution and ages of tectonic features that can be mapped on its surface (e.g., grabens and wrinkle ridges). For this investigation, 24,452 tectonic features of the western hemisphere of Mars (90°N to 90°S latitude and 0° to 180°W longitude) were mapped, digitized, and characterized using Viking images and 60 subquadrangle photomosaic bases at 1:2,000,000 scale; the data was then compiled into a workable spreadsheet. Each digitized structure consists of a pair of x-y references for its

beginning and ending points, which were converted into Martian coordinates for correlation and verification with the base maps. For simplification, curvilinear features were subdivided into multiple linear segments along natural breaks in trend. All data were carefully checked and verified for accuracy (*Anderson et al.,* 1998, 1999). The age of deformation for each feature was determined based on the established Martian stratigraphic column [*Tanaka,* 1986].

It is well established that grabens and rifts are bounded by normal faults that result from extensional stresses and that wrinkle ridges most likely formed by thrust faults and folds that result from compressional stresses (see review by *Banerdt et al.* [1992] and references therein). Because the surface of a planet is a free boundary (i.e., stress free), one of the principal stresses is vertical and the other two are horizontal near the surface in areas without extreme relief (*Anderson,* 1951). Under these conditions the type of fault that forms is directly related to the orientation of the principal stresses, and in particular, which principal stress is vertical. Normal faults or grabens form when the maximum principal stress, S_1, is vertical. The strike of a normal fault or graben represents the intermediate principal stress, S_2, and the minimum principal stress, S_3, is horizontal and perpendicular to the fault trace. For compressional structures, such as the faults and folds believed to make up wrinkle ridges, S_3 is vertical, S_1 is horizontal and perpendicular to the strike of the structure and S_2 is horizontal and parallel to the structure. Over an extended distance of a planet's surface the strike of a graben and the subsurface bounding faults both lie within the S_1 - S_2 plane (i.e., the plane perpendicular to S_3), which is everywhere vertical at the planet's surface (along the grabens trace) and if extended would intersect the center of the planet. The only plane that has this geometry is a great circle of a net that is parallel to the strike of the graben. The normal to a wrinkle ridge lies within the S_1 - S_3 plane (i.e., the plane

perpendicular to S_2). This plane is perpendicular to the surface of the planet and parallel to the surface normal of the ridge, so if extended it would intersect the center of the planet. The only plane that has this geometry is a great circle of a net that is perpendicular to the ridge trace. As a result, this analysis has a physical basis in terms of the orientations of structural features over the surface of a planet and the orientation of the causative stresses within the planet's lithosphere.

If the stress field is circularly symmetric, then radial structures will have traces of their strike converge or intersect at the geometric "center" of the stress field. In contrast, concentric structures will have normals to their traces intersect at the geometric center of the stress field. In this paper, the term center refers to the primary geometric center of the stress field; "secondary centers" refers to additional areas with high concentrations of radial structures that are statistically significant, but may or may not be geologically significant. In this study, two similar quantitative analytical techniques are applied to the comprehensive dataset to identify regional centers of tectonic activity in the western hemisphere of Mars: beta and vector analysis.

Beta Analysis

Beta analysis is a common technique used in structural geology to derive the intersection lines of a number of planes in three dimensions, such as determining the fold axis from the strike and dip of bedding around the fold hinge. To perform a beta analysis, the great circle planes of bedding are plotted on a stereonet and the intersection points of the planes are typically contoured to define the fold axis. This is mathematically equivalent to defining the great circle plane that contains a structure (or its perpendicular) on the surface of a planet and determining the intersections of these planes. Part of the problem for carrying out this type of analysis for large data sets is that the number of intersections of great circles on a net is n(n-1)/2, where n is

the number of great circles. Contouring by hand therefore becomes impossible for any but small data sets. However, the analysis of the intersection points of traces of great circles on a net is identical to the beta analysis of lines produced from the intersection of planes on a net in structural geology, for which computer contouring programs exist. For this analysis a published FORTRAN program (Beasley, 1981) was modified to take the information defining the great circle planes and iteratively count their intersections on a net with the percentage density of intersections in finely divided 1.0% counting areas. Contouring the intersections emphasizes their maximum concentrations. Areas of highly concentrated intersections represent candidate centers of the causative stress field.

The pattern of the contoured intersections can then be used to gauge how well the set of tectonic features is radial about a point. For example, a circular "bull's eye" pattern with one central concentration maximum of high density is a good indication of a radial distribution. The center of the maximum concentration pattern is simply the center of the radial data set. In contrast, an asymmetric density pattern with no central maximum or a number of smaller density concentration maxima indicates a non-radial system. Note that the results of a beta analysis are comparable to those of a pi analysis, in which the poles of the great circles are plotted directly on the net and contoured. In this analysis, a radial distribution is defined by a girdle of the poles. Ideally, these poles would lie along a perfect great circle or girdle (if poles to structures in one half of the region are arbitrarily inverted), whose pole would define the center of the radial system. The advantage of the pi analysis is that the total number of data points is simply the number of great circles, rather than the n(n-1)/2 of the beta analysis. However, accurately defining a single great circle from a contoured girdle pattern derived from a large data set with many arbitrarily inverted poles is very difficult, involving errors of order tens of degrees.

Although the beta analysis produces a large data set, the center of a contoured intersection plot of radial great circles is straightforward to define, and the results are directly interpretable in terms of the center of a system of radial faults on the surface of a planet and the causative stress system over the entire faulted surface of the planet.

Vector Analysis

A similar method for identifying radial centers of tectonic activity is to project structural features as vectors (*Anderson and Peer,* 1995) defined from their surface traces (and the center of the planet). This method is similar to constructing beta diagrams (using great circle projections) where the length and orientation for each structure is determined from the digitized beginning and ending points (or its perpendicular for wrinkle ridges). For this study, a 180 by 180 (1°) grid was established. Each structure was projected as a great circle and the number of structures radial to each grid point was counted. The counted number of structures radial to the grid points were then contoured. The largest concentration of radial structures is used to identify the primary center of radial activity and the center of the causative stress field for each stage. In this paper, results obtained from the vector method were converted into percent of the total number of structures for comparison with the results obtained from the beta analysis.

Structural Classification

Each mapped feature was classified according to relief and morphology (Table 1) based on the review by *Banerdt et al.* [1992]. Features that formed by extensional stresses were grouped into four main categories: simple grabens, complex grabens and rifts, tension cracks, and structural troughs/channels. These features were further divided into subcategories based on

structural type, size, morphology (e.g., indication of possible subsequent modification), or its spatial relation to nearby structures [*Anderson et al.,* 1997].

Simple Grabens (Figure 2a): Most of the structures identified in this study were classified as simple grabens. Simple grabens are long (tens to hundreds of kilometers) and narrow (less than five kilometers in width) troughs bounded by inward dipping normal faults with relatively flat floors and smooth fault scarps [e.g., *Tanaka and Davis,* 1988, *Tanaka et al.,* 1991, *Davis et al.,* 1995]. In places, these features are associated with pit crater chains (Figure 2b).

Complex Grabens and Rifts (Figure 2c): Complex grabens have widths that generally range between 10 and 100 kilometers and depths up to a few kilometers. These structures are characterized by complex, multiply faulted borders and floors [e.g., *Plescia and Saunders,* 1982] and generally resemble large, complex rift systems on Earth [*Banerdt et al.,* 1992].

Tension Cracks: Tension cracks and joints are morphologically distinct from simple grabens in that they are typically narrow, deep structures or grooves (Figure 2d) without identifiable flat floors [*Schumm,* 1974; *Tanaka and Golombek,* 1989; *Banerdt et al.,* 1992]. In places, tension cracks appear to be associated with pit crater chains and simple grabens with pit chains, which appear to be volcanic (Figure 2b) [e.g., *Tanaka and Golombek,* 1989*; Mege and Masson,* 1996a].

Troughs/Channels: Other mapped features that were included in this dataset, which may have formed by extensional tectonism, include the large Valles Marineris troughs [e.g., *Blasius et al.,* 1977*; Lucchitta et al.,* 1992; *Mege and Masson,* 1996b; *and Schultz,* 1998], nonbranching valleys, structurally controlled sapping channels [e.g., *Davis et al., 1995*], and troughs of polygonal patterned ground [e.g., *Pechmann,* 1980, *McGill,* 1986]. Because some of these

features may not be tectonic in origin, only the large Valles Marineris troughs that are clearly tectonic in origin were included in the subsequent analyses.

Wrinkle Ridges: Wrinkle ridges are complex linear to arcuate asymmetric topographic highs (Figure 2e) that are found primarily on smooth plains [e.g., *Chicarro et al.,* 1985, *Watters and Maxwell,* 1986, *Watters,* 1988]. Although a variety of volcanic and tectonic origins have been suggested for wrinkle ridge formation, most recent work, which includes the identification of a number of Earth analogs, has shown that they result from compressional faulting and folding of surface units [e.g., *Golombek and Plescia,* 1986; *Watters,* 1988, 1993; *Golombek et al.,* 1991]. In this study, wrinkle ridges were mapped, digitized and separated into there own class; ridges were not broken down into subclasses according to morphology. Previous work shows that wrinkle ridges formed in the Early Hesperian (Stage 3 of this study) [*Scott and Dohm,* 1990a, *Tanaka et al.,* 1991, *Watters,* 1993]. In this study, we performed vector and beta analyses on Stage 3 features with and without the addition of wrinkle ridges to identify primary centers.

Regional Age Correlation

Stratigraphic and crosscutting relations among stratigraphic/morphologic units permitted us to construct a map of the faults and grabens as they formed during five successive stages based largely on the age classification scheme of *Dohm and Tanaka* [1999]. The five stages are defined by major periods of geologic activity, which are recorded in the stratigraphic units identified for the western equatorial region [*Scott and Tanaka,* 1986], Alba Patera [*Tanaka,* 1990], Olympus Mons [*Morris and Tanaka,* 1994], Valles Marineris [*Witbeck et al.,* 1991], and Thaumasia regions [*Dohm and Tanaka,* 1999] (Table 2). Similar methods were used for unraveling the tectonic histories of the Syria Planum [*Tanaka and Davis,* 1988], Tempe Terra

and Ulysses Patera [*Scott and Dohm,* 1990b], Alba Patera [*Tanaka,* 1990], and Thaumasia regions [*Dohm and Tanaka,* 1999] of Mars.

Each unit was assigned a stage based on crater densities, stratigraphic and structural relations within the Martian stratigraphic column [*Tanaka,* 1986] and on previously identified families of faults for the regions described above. We show slight overlaps in the stratigraphic age of each fault stage, based on uncertainties in the stratigraphic age of the units. The stages are: Stage 1, Noachian; Stage 2, Late Noachian to Early Hesperian; Stage 3, Early Hesperian; Stage 4, Late Hesperian to Early Amazonian; Stage 5, Middle Amazonian to Late Amazonian. The stage assignments of structures on the maps adhere to the following guidelines: (1) structures of younger age may extend across boundaries of older units, (2) structures of intermediate age may extend into older units but not into younger units, and (3) Stage 1 structures occur only in Noachian units. However, some structures that are wholly confined to their host units and not in contact with younger units are indeterminate in age and are assigned the age of the host unit, even where previous workers assigned younger ages to these faults based on their similar orientation and morphology to nearby faults. For most features, the stage and age dates were the same. The major differences appear to be associated with faults around Alba Patera and in Sirenum and Memnonia. For example, the complex system of faults radial to and deflected about Alba Patera consists of graben and fault segments, which are wholly confined in places, to Early Hesperian host units. Although these segments are assigned an Early Hesperian age (Stage 3), they may have been formed or reactivated concurrently with similar-trending faults and grabens that cut younger materials of Late Hesperian age (Stage 4).

Statistical Significance and Uncertainty

Two types of uncertainty affect our analyses: the statistical significance of a given radial center and the spatial uncertainty of its location. In this paper, a center is defined by its location, the number of great circle intersections or structures projected that are radial to it, and its statistical significance from a random distribution at some confidence level. A variety of tests have been devised to test the significance of a concentration of data points on a contoured density diagram (e.g., see review by *Stauffer* [1966] and references therein]. Subsequent work has shown that a simple and intuitive test developed by *Kamb* [1959] is a reasonable method of estimating the statistical significance of a concentration of points on a contoured density diagram [e.g., *Dudley et al.*, 1975, *Robin and Jowett*, 1986, *Jowett and Robin*, 1988]. The significance level is defined relative to a random distribution over the hemisphere considered, and is:

$$(1) \qquad \sigma^2 = N\,A\,(1\text{-}A)$$

where σ^2 is the variance, N is the total number of structures or intersections in the diagram, and A is the relative area of the window used to count great circle intersections or projected radials to structures, which is typically 1%. This test basically assumes that a departure, in terms of the standard deviation (*Kamb* [1959] suggested 3σ), for a randomly extracted point count from a uniform parent population is statistically significant. Although subsequent work has shown that there is no statistical theory that assesses the statistical significance of a cluster of data points on a contoured density diagram [e.g., *Dudley et al.*, 1975, *Jowett and Robin*, 1988], an empirical statistic can be used that is similar to the *Kamb* [1959] test (but can be performed for much smaller than 1% counting areas). The probability that a given concentration of points is

statistically significant at the 95% confidence level is [*Jowett and Robin,* 1988, *Robin and Jowett,* 1986] is:

(2) $P_{95} = \exp[.053(\ln N)^2 + 0.434]$

and is roughly equivalent to the *Kamb* [1959] test at higher standard deviations (7.4σ due to the larger population of points in our plots [see *Jowett and Robin,* 1988]). Table 3 is a list of primary and secondary centers identified from the vector and beta techniques, where N refers to the number of extensional features identified per Stage; Center name is the reference name given for each center at the center point identified from the vector method, V_c^* and the beta analysis, B_c; the number (and percentage of the total) of structures radial within 1° of the center, N_r^V; the Gaussian peak statistic at the 95% confidence level, P_{95} to which N_r^V should be compared; the total number of great circle intersections, N^B, for N; the maximum number (and percentage of the total) of great circle intersections within a 1% counting area, N_i^B, defining B_c; the 3σ and 7.4σ *Kamb* statistic to which N_i^B should be compared, $E_k(N^B)$; the number of radial structures, N_r^B, that make up N_i^B; and the 3σ and 7.4 σ *Kamb* [1959] statistic to which N_r^B should be compared, $E_k(N)$. The reason the number of structures making up N_r^V is much smaller than N_r^B is that the vector method counts radial structures in an area (1° radius) that is a factor of 20 smaller than the beta method (1% area). As a result, N_r^V concentrations can be compared to the P_{95} *Jowett and Robin* [1988] statistic, which is identical to the *Kamb* [1959] statistic for these smaller counting areas. The reason that N_r^B is not exactly 20 times greater than N_r^V is that the N_r^V drops off to lower levels around the peak reported in Table 3 (tests of a number of centers shows that N_r^V is close to N_r^B for the equivalent counting area). Calculation of the *Kamb* [1959] E_k statistic for the smaller 1° radius counting area of the vector method yields significance levels equivalent to a factor of 20 lower than $E_k(N)$ shown, which are all lower than the the P_{95} *Jowett*

and Robin [1988] statistic shown for each stage. Table 3 shows that all primary and secondary centers defined are significant at the 95% confidence level of not resulting from a random distribution of points. In fact, all calculated centers have concentrations of points that so far exceeds random distributions that they are also significant at the 99% confidence level [e.g., *Jowett and Robin,* 1988] and therefore indicate that the calculated centers represent real centers to which radial structures project.

The spatial uncertainty of a projected center location is ±2°. This was estimated from a Monte Carlo test on several synthetic data sets with the vector program. The test data consisted of 8 to 24 structures arranged around a predetermined center. The Monte Carlo procedure consisted of calculating the center for the data with normally distributed (0.5 degree variance) random shifts applied to each structure. The center was calculated 1000 times for randomized structure sets producing a scatter with a full width half mean of 4°. We expect the main source of uncertainty to be geodetic errors in the martian cartographic grid system, but these errors should lie within 0.5 mm (1 km) of their published location (within the control net of *Davies, et al.* [1978]). Errors associated with tracing the features on the maps are certainly similar and likely less than ±5 km (±0.08°) for each end point. Other sources of positional uncertainties include our assumption of a spherical planet for center projection with both vector and beta programs, although the variation of the center position showed little or no variation with latitude in our analyses.

Data Analysis and Observations

Structural Types

Of the 24,452 tectonic structures mapped, 19,898 were mapped as extensional features and 4,554 were mapped as compressional features. Of the extensional features, 81% are simple grabens, 12% are tension cracks, and 7% are troughs and channels (Table 1).

Structural Age

Figure 3 shows the total number of extensional features mapped by stage and type of structure. Approximately half of the structures identified are Stage 1 (45%), 8% are Stage 2, 18% are Stage 3, 17% are Stage 4, and 6% are Stage 5. It is evident that simple grabens are by far the dominant structure found on Mars (Table 1). The number of simple grabens with respect to other extensional tectonic features during each stage decreases with time (Figure 3b), with stage 1 displaying the greatest percentage of simple grabens (74%).

Centers of Tectonic Activity

Figures 4a and b are vector and beta contour plots (centered on 90°W and the equator) derived from all extensional features in the western hemisphere of Mars. From both of these maps, a broad north-south, elongated "bulls-eye" pattern with a maximum concentration of intersections of just under 10% of the total of just under 200 million, indicate a generally radial distribution of extensional structures. The north-south elongation of the contour pattern probably results from the dominance of generally north-south trending structures located in the northern and southern regions of Tharsis (Figure 1). These regions have the most complete record of deformation, with many structures likely buried by younger materials to the east (e.g., Lunae, Syria and Solis Plana) and to the northwest (e.g., Tharsis lavas and Amazonis Planitia) of the Tharsis rise. This is evident by a rounding of the contour patterns when the compressional

features (e.g. wrinkle ridges) data were combined to the extensional features (Figure 5a, b). For the extensional features, two different primary centers were identified (Table 3): Claritas (vector) and Syria (beta), although the total difference in structures radial to Claritas versus Syria in the vector method is only 47 or 3.5%. When the two datasets were combined, both the vector (Figure 5a) and the beta (Figure 5b) identified the center of the radial structures (4°S, 107°W) to be located near Syria Planum (Figure 4b; Figure 5a, b). This region is also the center of the Tharsis topographic high, outside of the volcanoes [*Smith et al.*, 1999], which generally corresponds to the center of the stress field calculated for all of Tharsis [e.g., *Banerdt et al.*, 1992]. Secondary centers at Claritas, Syria, Alba and Ascraeus identified in the analyses of all structures and all extensional structures (Figures 4a and 5a, and Table 3) include the primary centers identified in for 4 of the individual stages discussed next.

Primary centers and secondary radial centers of tectonic activity identified from the vector and beta programs for the western hemisphere of Mars for each of the 5 stages of tectonic activity are listed in Table 3.

Stage 1: Stage 1 extensional features (Figure 6a) are primarily found in Noachian heavily cratered terrain around the periphery of and in small central outcrops within Tharsis in Sirenum, Claritas Fossae, Ceraunius Fossae, Tempe Terra, Acheron Fossae, and northern part of Noctis Labyrinthus. From the vector analysis of Stage 1 data (Figure 6b), a broad center (elongated "bulls-eye" or "girdle") of tectonic activity (Claritas) was identified at 27°S, 106°W (815 Claritas-centered radial features or 9% of the Stage 1 data). A similar center (14°S, 106°W) and contour pattern (Figure 6c) was identified by the beta program (beta analysis: 9% or 40,230,226 intersections). Although the two methods varied by 12° latitude in identifying the location of the primary center, the results from both methods clearly demonstrate that this center is contained

within a broad geographic region between 30°S and 10°S along the 106°W longitude. The number of structures radial to the ten highest concentration counting bins within this region using the vector method varies by less than 5% (Table 4). Two additional statistically significant secondary centers were identified from the vector analysis method for Stage 1 features in southwest Tempe (35°N, 81°W,), and Uranius (24°N, 90°W).

Stage 2: Stage 2 extensional features (Figure 7a) are largely concentrated in Thaumasia and Valles Marineris where Late Noachian-Early Hesperian units have been mapped. These features project to a center, which is located south of the central margin of Valles Marineris (Valles) using vector (16°S, 77°W; Figure 7b) and beta (12°S, 78°W ; Figure 7c) analyses. The beta analysis indicates that 12.8% of the Stage 2 extensional features intersect (1,242,160 intersections) in a reasonably circular "bulls eye" area. The vector analysis indicates that 13.1% of the Stage 2 features (207) are radial to the Valles center and the mapped pattern of concentrations of radial centers is much more diffuse. A secondary center of tectonic activity is located from both the vector and beta analysis in the source region of Warrego Valles (35°S. 96°W).

Stage 3: Stage 3 extensional structures occur primarily in Thaumasia, Tempe Terra, Ulysses, Noctis Labyrinthus, and Valles Marineris (Figure 8a) where Early Hesperian units are mapped. A primary center is located in the northwestern part of Syria Planum in Noctis Labyrinthus (4°S, 107°W) using the vector (Figure 8b) and beta analyses (Figure 8c; 3°S, 108°W). The beta analysis indicates that 11.9% of the Stage 3 extensional features intersect (10,102,108 intersections) at the identified center in a reasonably circular "bulls eye" pattern; while vector analysis shows 8.4% (379 NW Syria centered radial features) at the same center within a more diffuse "girdle" distribution of radial features. Secondary centers were identified

by the vector analysis at Syria (19°S, 104°W), Pavonis (6°N, 114°W), Tempe SW (30°N, 80°W), and Ulysses (10°N, 124°W) regions.

Wrinkle ridges are found primarily in the ridged plains materials that are dated as Early Hesperian in age [*Watters,* 1993], which corresponds to Stage 3 of this study. Wrinkle ridges are concentrated in Lunae and Solis Plana to the east of Tharsis, although lesser concentrations are also found to the west (Figure 6a). Figures 9b and 9c are contour plots of perpendiculars to wrinkle ridge strikes derived from vector and beta analyses. Results of both methods show a diffuse zone of concentrations that is made up of one or two girdles [*Anderson et al.,* 1999], which does not define a very good radial distribution. This elongate concentration of wrinkle ridge perpendiculars has been noted previously by *Wise et al.* [1979] and by *Watters* [1993] and shows that wrinkle ridges are not concentric about a single point. Two elongate concentrations stretching from 15°S, 95°W to 4°N, 125°W and a smaller linear area centered around 20°N and ranging from 40°to 70°W may represent secondary centers. The location of the centers are in general agreement with one elongate center identified by *Wise et al.* [1979] and both those identified by *Watters* (1993) using beta analysis on smaller data sets (which explains the differences in the concentrations derived). When normals to wrinkle ridges are combined with the Stage 3 extensional structures (Figure 10a, b), the same Syria center for the extensional structures (Figure 8b) is found as the primary center (4°S, 107°W). The beta analysis shows a reasonable "bulls eye" pattern of intersections indicating a radial distribution, although the vector method does show a more diffuse pattern with multiple secondary centers.

Stage 4: Stage 4 extensional features occur in Late Hesperian-Early Amazonian units in Alba Patera, Tempe Terra, and around Olympus Mons and the Tharsis Montes (Figure 11a). Vector and beta analyses of the Stage 4 extensional features (Figures 11b and 11c respectively)

identify a broad center of structures radial to Alba Patera, where most of the structures are located. The primary center of structures identified in the beta analysis—at 42°N, 104°W, comprising 10.3% of the features or 6,716,066 intersections occurs in an elongate "bulls eye" pattern, whereas the vector center at 37°N, 107°W, comprising 9.8% or 358 radial features, occurs in a more diffuse "girdle. This elongated pattern is likely due to the dominance of north-south oriented structures around Alba.

Stage 5: Stage 5 tectonic activity is largely observed around the large shield volcanoes, Ascraeus, Arsia, Pavonis, and Olympus Mons (Figure 12a) and other Middle to Late Amazonian volcanics on top of Tharsis. A reasonably circular "bulls eye" center identified from the vector (8°N, 106°W) and beta analyses (7°N, 106°W --Figures 12b and 12c, respectively) is located to the northeast of Pavonis Mons. The beta analysis shows that 13.7% of the Stage 5 extensional features intersect (703,613 intersections) at this location, whereas vector analysis shows 17.5% (207 radial features), with contours defining elongate concentrations to the north and northwest A possible secondary concentration of radial structures appears in the Beta analysis near Olympus Mons at roughly 25°N, 135°W.

Discussion

The paleotectonic maps presented in this paper show that the Tharsis province as defined by its tectonic features has been active throughout recorded Martian geologic time (from the Noachian through Late Amazonian). Judging by the number of tectonic features presently observed at the surface, Tharsis related activity began early and has generally decreased with time. Analysis of the spatial distribution of structures throughout time shows that the province has generated statistically significant concentrations of radial structures throughout geologic

time. The geometric center of these structures has moved but has always remained centered on the higher elevation regions of the province [*Smith et al.*, 1999]. Taking all the structures together shows they are radial to the highest part of Tharsis outside of the volcanoes, near Syria Planum. This result is generally consistent with previously defined centers by *Wise et al.* [1979] and the combined two main centers [*Golombek,* 1989] defined by *Plescia and Saunders* [1982]. Lithospheric stress models of the Tharsis province, based on the present global topography and gravity of Mars also show stress fields that are centered near Syria Planum [e.g., *Banerdt et al.*, 1992]. The calculated stress fields appear capable of generating the radial pattern of structures [*Banerdt and Golombek,* 2000], so to first order, the geometry of the structures agrees with the calculated stress fields. This agreement actually suggests that the basic lithospheric structure of the province has not changed much since the Hesperian (Stage 3), given that stress models are based on present day topography and gravity.

More than half of the mapped extensional features in the western hemisphere region are Noachian (Stage 1); they are most abundant in the Syria Planum, Thaumasia, and Tempe Terra regions. Many of these features are radial to Claritas, a large elongated topographic high, which contains numerous simple and complex grabens that were formed and (or) reactivated over a large period of time (Noachian-Amazonian; see *Dohm and Tanaka* [1999]). This center represents the oldest identifiable center of tectonic activity for the western hemisphere of Mars and corresponds to the early phase of Thaumasia faulting discussed by *Frey* [1979] and *Plescia and Saunders* [1982]. In addition to the Stage 1 Claritas center, additional tectonic activity was identified at Tempe and Uranius (predating the relatively young shield volcano and associated lava flows). The two secondary concentrations in the Tempe Terra region (Figure 6b) may be

related to previously identified deep-seated intrusives in this area [*Scott and Dohm,* 1989; Anderson and Dohm, 2000].

During the Late Noachian and Early Hesperian (Stage 2), radial tectonism was centered just to the south of the central margin of Valles Marineris. Intrusive-related activity within the Valles Marineris region [*Lucchitta,* 1992] and possible associated outflow channel development [e.g. *Dohm et al.,* 1998b; *McKenzie and Nimmo,* 1999] may be related to this tectonic activity. *Schultz* [1998] suggests that Valles Marineris largely formed during the Late Hesperian and Early Amazonian (Stage 4 activity of this study), but geologic evidence in the Thaumasia region [*Dohm and Tanaka,* 1999] and elsewhere indicates that Valles-related fault development may have occurred as early as the Late Noachian (Stage 2). Valles-centered radial Stage 2 grabens, for example, are buried by Stage 3 lavas in the Thaumasia region. A Stage 2 secondary concentration occurs at the source region of Warrego Valles, which has been interpreted to be a site of tectonic and intrusive-related hydrothermal activity resulting in the formation of Warrego Valles [*Dohm et al.,* 1998a]. It is possible that some structures radial to Stage 2 centers were active during Stage 1, but they may have been masked or reactivated by Claritas center structures (Stage 1).

During the Early Hesperian (Stage 3), continued tectonic activity occurred in Pavonis, Syria, Ulysses, and Tempe Terra regions. The Syria center defined by this investigation includes all the Pavonis centered structures defined by Plescia and Saunders [1982]. Syria Planum has been identified as a region of long lived (Noachian to perhaps Early Amazonian) volcanic and tectonic activity [*Tanaka and Davis,* 1988; *Tanaka et al.,* 1996; *Dohm and Tanaka,* 1999]. Wrinkle ridges also formed during Stage 3 [*Scott and Dohm,* 1989; *Watters,* 1993; *Tanaka et al.,* 1991]. Stage 1-3 structures also generally agree with the Late Noachian-Early Hesperian phase

of Tharsis activity identified by *Tanaka et al.* [1991], with the possible exception of distal radial faulting in Memnonia, Sirenum, and Thaumasia which occur in Noachian and Early Hesperian units and so are classified as Stage 1, 2 and 3 structures herein, but which all could have formed Stages 2 and 3 (see earlier discussion on age correlation).

Tectonic activity centered at Alba Patera dominates the Late Hesperian (Stage 4). During this time, voluminous sheet lavas were emplaced in Syria Planum to the south, and outflow channel development, possibly related to late-stage activity at Valles Marineris, was occurring to the east. This period also includes the first appearance of the large shield volcanoes of Tharsis Montes and Olympus Mons, and late-stage activity related to the Tempe center. During Stage 5, there is a reduction in the number of simple grabens and isolated occurrences of tectonic activity associated with continuing construction of the large Tharsis shield volcanoes. Other than minor graben formation associated with the final stages of Alba Patera, these local volcanic sources may represent late-stage pulses of tectonic activity for the Tharsis region. Stage 4 and 5 structures agree with those identified by *Tanaka et al.* [1991] for the second main phase of Tharsis activity and corresponds to the Pavonis II phase of faulting identified by *Plescia and Saunders* [1982].

Conclusion

1) The orientation of 24,452 structures in the western hemisphere of Mars form a statistically significant radial and concentric pattern around Syria Planum, the highest part of Tharsis, outside of the volcanoes.
2) Detailed mapping of these structures in the established stratigraphic framework of Mars shows that they formed during 5 main stages beginning in the Noachian and extending

through the Amazonian. Over half of the tectonic features presently preserved on the surface are Noachian in age, arguing that tectonic activity peaked early and generally decreased with time.

3) Because flexural loading lithospheric stress models in the literature based on present gravity and topography can explain the observed radial distribution of structures, the basic lithospheric structure of the province has probably changed little since the Noachian.
4) Structures formed in the Noachian (Stage 1), predominantly in Syria, Thaumasia, Uranius and Tempe are radial to Claritas, a large north-south ridge covering 20° in latitude. Secondary radial distributions of structures are found in Tempe and Uranius.
5) Structures that formed during the Late Noachian/Early Hesperian (Stage 2) are concentrated along the present trend of Valles Marineris and in Thaumasia and are radial to a location just to the south of the central margin of Valles Marineris. A subset of Stage 2 structures forms a radial pattern around Warrego Valles in the Thaumasia region.
6) Early Hesperian (Stage 3) extensional structures in Pavonis, Syria, Thaumasia, Ulysses, Tempe, and northern Alba are radial to Syria Planum. Intersections to normals of wrinkle ridges, formed during Stage 3, in Lunae and Solis Plana, and in Sirenum, Memnonia and Amazonis are not radial about a single point, forming a diffuse single or double girdle pattern with 2 maxima . All extensional structures and wrinkle ridges together appear centered on Syria Planum.
7) Late Hesperian/Early Amazonian (Stage 4) extensional structures in Alba, Tempe and the Tharsis volcanoes appear radial to Alba Patera, which dominated tectonic activity during this period.

8) Middle to Late Amazonian structures (Stage 5) represent the waning phases of tectonic activity on Mars. These structures are associated with the large volcanic constructs and are radial to an area northeast of Pavonis Mons.

9) Statistically significant secondary centers of radial structures formed during all of the stages. Many of these secondary centers appear related to previously identified local magmatic centers that formed at different times and locations throughout.

REFERENCES

Anderson, E.M., The dynamics of faulting, 2nd ed., 206 p., Oliver and Boyd, Edinburgh, 1951.

Anderson, R. C., Lineament analysis and tectonic interpretation for the central tharsis region, Mars. *Lunar Planet. Sci.*,, XIX, page 12, (abstract), 1988.

Anderson, R.C. and Peer, B.J., An analytical approach to identifying radial lineaments associated with the Tharsis Region of Mars. *Lunar Planet. Sci.*, XXV, page 41, (abstract), 1995.

Anderson, R.C., Golombek, M.P., Franklin, B.J., Tanaka, K.L., Dohm, J.M., Lias, J., and Higdon, J., A new detailed structural history of the Tharsis Region of Mars, *Lunar Planet. Sci.*, XXVIII, P. 39-40, (abstract), 1997.

Anderson, R.C., Golombek, M.P., Franklin, B. J., Tanaka, K. L., Dohm, J. M. , Lias, J. and B. Peer, Significant centers of tectonic activity through time for the western hemisphere of mars, *Lunar Planet. Sci.*, XXIX, P. 1881-1882, (abstract), 1998.

Anderson, R.C., Haldemann, A.F.C., Dohm, J.M., Golombek, M.P., Franklin, B.J., and J.Lias, Significant centers of tectonic activity as identified by wrinkle ridges for the western hemisphere of mars, *Lunar Planet. Sci.*, XXX, (abstract), 1999.

Anderson, R.C., and Dohm, J.M., Magmatic-tectonic evolution of Tharsis, *Lunar Planet. Sci.*, XXXI, #1607, (abstract), 2000..

Banerdt, W.B., Golombek, M.P., and K.L. Tanaka, Stress and tectonics on Mars, Chapter 8, p. 249-297, *in* MARS, Kieffer, H. H., Jakosky, B. M., Snyder, C. W., and Matthews, M. S., eds., University of Arizona Press, Tucson, 1498 pp., 1992.

Banerdt, W.B., and Golombek, M.P., Tectonics of the Tharsis Region, Insights from MGS topography and gravity, *Lunar Planet. Sci. Conf.*, XXXI, #2038, (abstract), 2000.

Beasley, A.J., A computer program for printing geometrically accurate structural fabric diagrams, *Computers & Geoscience,* 7, p. 215-227, 1981.

Blasius, K.R., Cutts, J.A., Guest, J.E., and H. Masursky, Geology of the Valles Marineris: First analysis of imaging from the Viking I Orbiter primary mission, *J. Geophys. Res.,* 82, p. 4067-4091, 1977.

Carr, M.H., Tectonism and volcanism of the Tharsis Region of Mars, *J. Geophys. Res.,* 79, 26, p. 3943-3949, 1974.

Chicarro, A.F., Schultz, P.H., and P. Masson, Global and regional ridge patterns on Mars, *Icarus,* 63, p. 153-174, 1985.

Davies, M.E., The Control Net of Mars: May 1977, *J. Geophys. Res.,* 82, p. 2311-2312, 1978.

Davis, P.A., Tanaka, K.L., and Golombek, M.P., Topography of closed depressions, scarps, and grabens in the north Tharsis region of Mars: Implications for shallow crustal discontinuities and graben formation. *Icarus,* 114, p. 403-422, 1995.

Dohm, J.M., Tanaka, K.L., Lias, J.H., Hare, T.M., Anderson, R.C., and Gulick, V.C., Warrego Valles and other candidate sites of local hydrothermal activity within the Thaumasia Region, Mars, *Lunar & Planet. Sci. Conf.,* XXIX, P. 1669, (abstract),1998a.

Dohm, J.M., Anderson, R.C., and K.L. Tanaka, Digital structural mapping of Mars, *Astron. & Geophys.*, 39, 3, p. 320-322, 1998b.

Dohm, J.M., and Tanaka, K.L., Geology of the Thaumasia region, Mars: valley, origins, volcanic evolution, and plateau development, accepted *Planet. & Space Sci.*, 1999.

Dudley, R.M., Perkins, P.C., and M.E. Gine, Statistical tests for preferred orientation, *J. Geology,* 83, p. 685-705, 1975.

Frey, H., Thaumasia: A fossilized early forming Tharsis uplift, *J. Geophys. Res.*, 84, 83, 1009-1023, 1979.

Golombek, M.P., Geometry of stresses around Tharsis on Mars, *Lunar Planet. Sci.*, XX, 345-346, (abstract), 1989.

Golombek, M.P., Plescia, J.B., and B.J. Franklin, Faulting and folding in the formation of planetary wrinkle ridges, *Proc. Lunar Planet. Sci. Conf.*, 21, p. 679-693, (abstract),1991.

Jowett, E.C., and Robin, P. -Y. F., Statistical significance of clustered orientation data on the sphere: an Empirical Derivation, *J. Geology*, 96, p. 591-599, 1988.

Kamb, W.B., Ice Petrofabric Observations from Blue Glacier, Washington, in relation to theory and experiements, *J. Geophys. Res.*, 64, p. 1891-1919, 1959.

Lucchitta, B.K., McEwen, A.S., Clow, C.D., Geissler, R.B., Singer, R.B., Schultz, R.A., and S.W.Squyres, The canyon system on Mars, In *Mars,* ed. H.H. Kieffer et al., p. 453-492, Univ. of Ariz. Press, Tucson, 1992.

McGill, G.E., The giant polygons of Utopia, Northern Martian Plains, *Geophys. Res. Lett.,* 13, p. 705-708, 1986.

McKenzie, D., and Nimmo, F, The generation of Martian floods by the melting of ground ice above dykes: *Nature*, v. 397, 231-233., 1999.

Mege, D., and P. Masson, A plume tectonics model for the Tharsis Province, Mars, *Planet. Space Sci.,* 44, No. 12, p. 1499-1546, 1996a.

Mege, D., and P. Masson, Amounts of crustal stretching in Valles Marineris, Mars, *Planet. Space Sci.,* 44, No. 12, p. 749-781, 1996b.

Morris, E.C., and Tanaka, K.L., Geologic maps of the Olympus Mons region of Mars, *U.S. Geol. Surv. Misc. Invest. Ser. Map, I-2327-B,* 1994.

Pechmann, J.C., The origin of polygonal troughs on the northern plains of Mars, *Icarus,* 42, p. 185-210, 1980.

Plescia, J.B., and R.S. Saunders, Tectonic history of the Tharsis Region, Mars, *J. Geophys. Res.,* 87, p.9775-9791, 1982.

Robin, P.-Y,F., and Jowett, E.C., Computerized density contouring and statistical evaluation of orientation data using counting circles and continuous weighting functions, *Tectonophysics,* 121, p. 207-223, 1986.

Schultz, R.A., Multiple-process origin of Valles Marineris basins and troughs, Mars, *Planet. Space Sci.*, 46, p. 827-834, 1998.

Schumm, S.A., Structural origin of large martian channels, *Icarus,* 22, p. 371-384, 1974.

Scott, D.H., and K.L. Tanaka, Geologic map of the western hemisphere of mars; scale 1:15M, *U.S. Geol. Surv. Misc. Invest. Ser. Map, I-1802-A,* 1986.

Scott, D.H., and J.M. Dohm, Chronology and global distribution of fault and ridge systems on Mars, *Lunar Planet. Sci.,* XX, p. 487-501, (abstract), 1989.

Scott, D.H., and J.M. Dohm, Evidence for multiple flooding episodes in Kasei Valles, Mars, *Lunar Planet. Sci.,* XXI, p.1115-1116, (abstract), 1990a.

Scott, D.H., and J.M. Dohm, Faults and ridges: historical development in tempe terra and ulysses patera regions of Mars, *Lunar Planet. Sci.,* XX, p. 503-513, (abstract), 1990b.

Smith, D.E., et al., The global topography of Mars and implication for surface evolution, *Science*, 284, p. 1495-1503, 1999.

Stauffer, M.R., An empirical-statistical study of three-dimensional fabric diagrams as used in structural analysis, *Can. Jour. Earth Sci.,* 3, p. 473-498, 1966.

Tanaka, K.L., The stratigraphy of Mars, *Lunar Planet. Sci.,* XVII, *J. Geophys. Res. Suppl.* 91, p.E139-E158, 1986.

Tanaka, K.L., Tectonic history of the Alba Patera-Ceraunius Fossae region of Mars, *Proc. Lunar Planet. Sci. Conf.*, 19, p. 515-523, 1990.

Tanaka, K.L., and P.A. Davis, Tectonic history of the Syria Planum Province of Mars, *J. Geophys. Res.,* 93, p.14,893-14,917, 1988.

Tanaka, K.L., and M.P. Golombek, Martian tension fractures and the formation of grabens and collapse features at Valles Marineris, *Proc. Lunar Planet. Sci. Conf.*, 19, p. 383-396, 1989.

Tanaka, K.L., Golombek, M.P., and W.B. Banerdt, Reconciliation of stress and structural histories of the Tharsis region of Mars, *J. Geophys. Res.*, 96, p. 15,617-15,633, 1991.

Tanaka, K.L., Dohm, J.M., and T.R. Watters, Possible coronae structures in the Tharsis region of Mars, *Lunar Planet. Sci.,* XXVII, p. 1315-1316, (abstract),1996

Watters, T.R., Wrinkle ridge assemblages on the terrestrial planets, *J. Geophys. Res.*, 93, p. 15599-15616, 1988.

Watters, T.R., Compressional tectonism on Mars, *J. Geophys. Res.*, 98, E9, p. 17,049-17,060, 1993.

Watters, T.R., and T.A. Maxwell, Orientation, relative age, and extent of the Tharsis plateau ridge system, *J. Geophys. Res.,*91, 8113-8125, 1986.

Wise, D.U., Golombek, M.P., and G.E. McGill, Tharsis province of Mars: geologic seqeunce, geometry, and a deformation mechanism, *Icarus*, 38, p.456-472, 1979.

Witbeck, N.E., Tanaka, K.L., and D.H. Scott, Geologic map of the Valles Marineris region, Mars (East Half And West Half): 1:2M, *U.S. Geol. Surv. Misc. Invest. Ser. Map, I-2010,* 1991.

Table 1 Categories of structural features mapped in the western hemisphere of Mars.

Extensional features	**Number**
Simple Grabens (flat, visible floor and smooth walls)	
1. Narrow simple grabens (0-5 km wide)	13,613
2. Wide simple grabens (>5 km wide)	124
3. Altered simple grabens (appear to be partly eroded or filled in)	2,206
4. Grabens with pit chains	112
Complex Grabens/Rifts	
5. Complex grabens (10-50 km wide, stepped sides)	49
6. Altered complex grabens (appear to be partly eroded or filled in)	5
Tension Cracks	
7. Narrow tension cracks (0-0.5 km wide)	111
8. Wide (modified) tension cracks (>0.5 km wide)	1,714
9. Tension cracks with pit chains	91
10. Tension cracks associated with volcanoes	521
Troughs/Channels	
11*. Structurally-controlled fluvial channels	337
12*. Structurally-controlled sapping valleys	148
13*. Structurally-controlled troughs	866
Compressional Features	
Ridges/Scarps	
14. Wrinkle ridges (Linear hills with crenulation, may branch, curve or imbricate)	4,556

*Because a majority of these features may not be tectonic in origin, only the features associated with the large Valles Marineris troughs were retained in the data set for analysis.

Table 2 Correlation of regional and provincial fault sets and stages in the Tharsis region.

Tharsis/Thaumasia [Dohm et al., 1997]	**Tempe** [Scott & Dohm, 1990]	**Alba** [Tanaka, 1990]	**Ulysses** [Tanaka & Davis, 1988]	**Syria** [Tanaka & Davis, 1988]
(1) Noachian	Noachian Stages 1-5	Stage I	None	Stages IA & IB
(2) Late Noachian - Early Hesperian	None	Stage II	Fault Set I	Stage IIA
(3) Early Hesperian	Hesperian Fault Set 1, 2, 3 + ridges	None	Fault Set 2, 3, & 4	Stages IIB, III1, III2, III3, IIA, IVA, IVB1, IVB2
(4) Late Hesperian - Early Amazonian	Amazonian Fault System	Stage III	Amazonian Fault Set 1	Stages V, VI1, VI2
(5) Middle - Late Amazonian	None	Stage IV	Amazonian Fault Set 2	None

Table 3 Primary and secondary centers identified from the vector and beta analytical techniques.

Stage	N	Center Name	V_c*	N_r^v (%)	P_{95}	B_c	N^B**	N_i^B(%)	$E_k(N^B)$§		N_r^B¶	$E_k(N)$§	
									3 σ	7.4 σ		3 σ	7.4 σ
Stage 1	8972				125		40,230,226		1893	4669		266	656
(Primary)		Claritas	27°S, 106°W	815 (9.1%)		14°S, 106°W		3,620,720 (9.0%)			2691		
(Secondary)		Tempe SW	33°N, 81°W	488 (5.4%)									
		Uranius	24°N, 90°W	419 (4.7%)									
Stage 2	1577				27		1,242,160		333	821		47	116
(Primary)		Valles	16°S, 77°W	207 (13.1%)		12°S, 78°W		158,997 (12.8%)			564		
(Secondary)		Warrego	35°S, 96°W	168 (10.7%)		42°S, 89°W,		> 74,530 (> 6%)			> 386		
Stage 3	4496				66		10,102,108		949	2341		134	331
(Primary)		Syria NW	4°S, 107°W	379 (8.4%)		3°S, 108°W		1,202,151 (11.9%)			1551		
(Secondary)		Tempe SW	30°N, 80°W	298 (6.6%)		30°N, 80°W		303,063 (3%)			779		
		Ulysses	10°N, 124°W	271 (6.0%)									
		Pavonis	6°N, 114°W	299 (6.7%)									
		Syria S	19°S, 104°W	328 (7.3%)									
Wrinkle Ridges	4554				67		10,349,700		961	2370		135	332
		Lunae E	18°N, 48°W	394 (8.7%)		~13°S, 48°W		620,982 (6%)			1114		
		Syria NW	4°S, 108°W	373 (8.2%)		7°S, 107°W		1,511,056 (14.6%)			1738		
Stage 3 + wr @	9050				133		40,946,725		1909	4710		268	662
(Primary)		Syria NW	4°S, 107°W	567 (6.3%)		8°S, 109°W		3,111,951 (7.6%)			2714		
Stage 4	3666				55		6,716,066		774	1909		109	269
(Primary)		Alba	37°N, 107°W	358 (9.8%)		42°N, 104°W		691,755 (10.3%)			1176		
Stage 5	1187				22		703,613		250	617		35	86
(Primary)		Ascraeus S	8°N, 106°W	207 (17.5%)		7°N, 106°W		96,395 (13.7%)			428		
(Secondary)		Olympus				25°N, 135°W		49,253 (7%)			231		
All Features	24452				359		298,894,115		5159	12726		725	1788
(Primary)		Syria NW	4°S, 107°W	1464 (6.0%)		3°S, 109°W		17,936,276 (6.7%)			5989		
(Secondary)		Claritas	20°S, 104°W	1446 (6.0%)									
		Alba	28°N, 108°W	1142 (4.8%)									
		Tempe	30°N, 82°W	1071 (4.4%)									
All Extensional Features	19896				278		197,916,660		4198	10355		590	1455
(Primary)		Claritas	20°S, 104°W	1339 (6.7%)									
(Secondary)		Syria NW	3°S, 107°W	1292 (6.5%)		4°S, 109°W		16,229,166 (8.2%)			5557		
		Tempe	30°N, 82°W	935 (4.7%)									
		Alba	34°N, 107°W	1026 (5.2%)									
		Ascraeus N	14°N, 109°W	1164 (5.9%)									
		Ceraunus	22°N, 109°W	1163 (5.9%)									

Where: N is the total number of radial features; V_c is the geographic location of the center identified from the vector analysis (lat/long); N_r^v (%) is the number of radial features defining the center (also given as % of N) ; P_{95} is the Jowett and Robin [1988] Gaussian peak statistic for 95% confidence level, to which the N_r^v values should be compared; B_c is the geographic location of the center identified from the beta analysis (lat/long); N^B is the total number of intersections derived by the beta analysis program from N; N_i^B is the number of intersections (also given as % of N^B) that determine the center; $E_k(N^B)$ is the expected value for the Kamb [1959] method significance level relative to the population of intersections to which the N_i^B values should be compared; 3σ is Kamb's [1959] 95% confidence level and 7.4σ is Jowett and Robin's [1988] correction to Kamb [1959] (E+4.4σ); N_r^B is the number of radial features derived from N_i^B; $E_k(N)$ is the expected value for the Kamb [1959] method relative to the population of radial features to which the N_r^B values should be compared.

* Based on a one degree radius solid angle sample circle.

** N^B is not equivalent to N(N-1)/2 because of round-off error in the beta analysis program.

§ E_k is determined using equation (1).

¶ N_r^B is taken as the nearest integer to $(2\,N_i^B)^{1/2}$ as an approximation to $N_i^B = N_r^B(N_r^B-1)/2$.

@ Dataset contains all of Stage 3 features plus wrinkle ridges.

Table 4 Number of structures radial to the next ten highest concentration counting bins in the vector method for Stage 1 faults radial to Claritas.

Center	Latitude (degrees)	Longitude (degrees)	Number of Structures
1.	-26 S	-106 W	815
2.	-27 S	-106 W	803
3.	-29 S	-106 W	791
4.	-25 S	-106 W	789
5.	-28 S	-106 W	786
6.	-28 S	-107 W	776
7.	-27 S	-107 W	774
8.	-20 S	-104 W	768
9.	-29 S	-107 W	765
10.	-26 S	-107 W	764

Figure 1 Paleotectonic map of the Western Hemisphere of Mars. Color correspond to stratigraphic age of the tectonic features as shown. Wrinkle ridges are in Stage 3. Symbols represent regions around Tharsis that are discussed in the text: Acheron Fossae (AF), Alba (A), Tempe Terra (TT), Ceranius Fossae (CF), Tharsis Montes (TM), Lunae Planum (LP), Noctis Labyrinthus (NL), Syria Planum (S), Valles Marineris (VM), Claritas Fossae (CIF), Thaumasia (Th) , Memnonia Fossae (MF), Sirenum Fossae (SF), and Warrego (W). Numbers represent centers identified from this study.

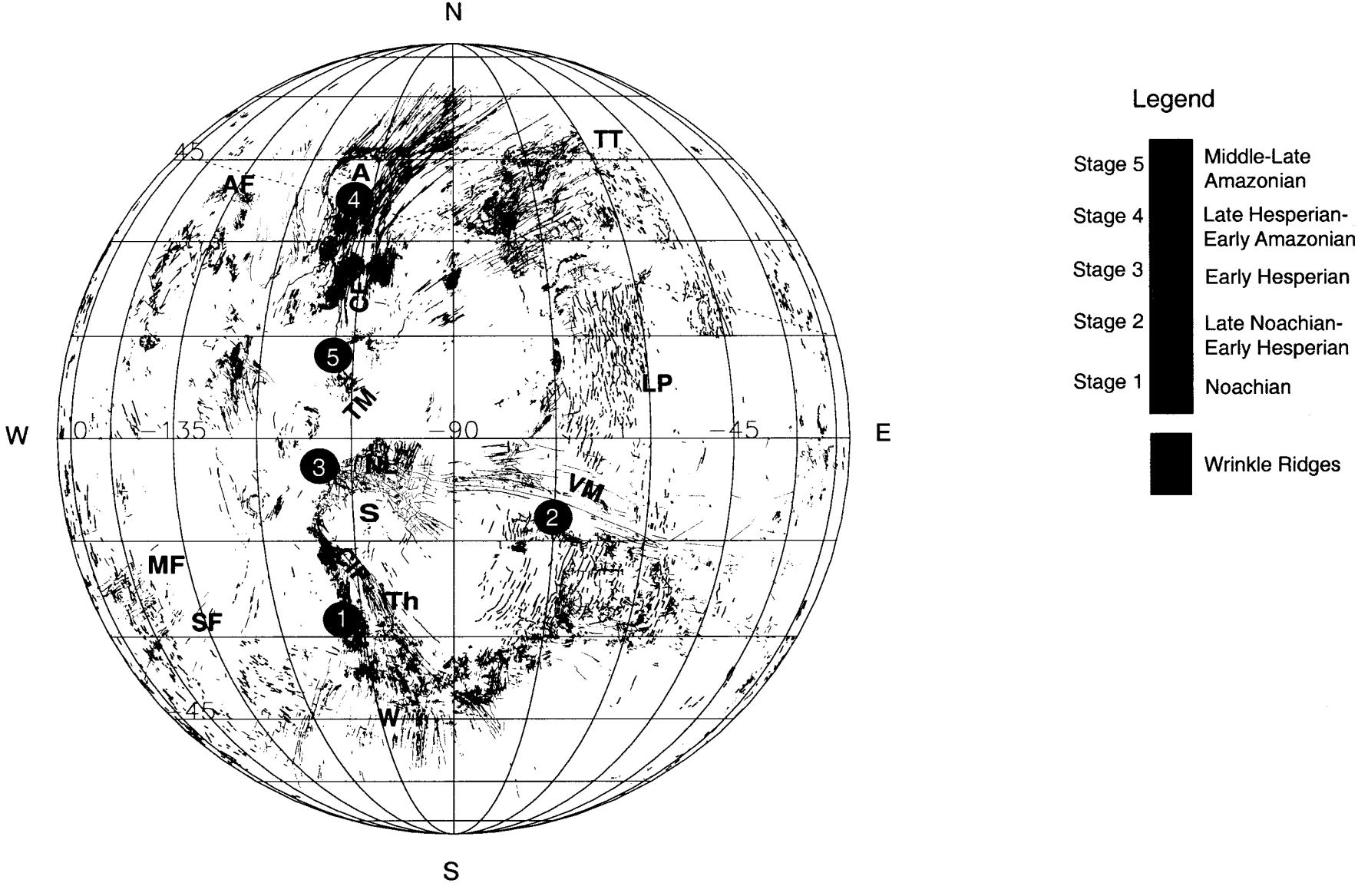

Figure 2a Fresh, Amazonian age simple graben on Solis Planum of Mars (30 ^{o}N, 95 ^{o}W). Arrows in this and subsequent figures denote north. The graben has a flat floor, smooth walls and is less than 10 km wide. (Mars Digital Image Map, MI30S092).

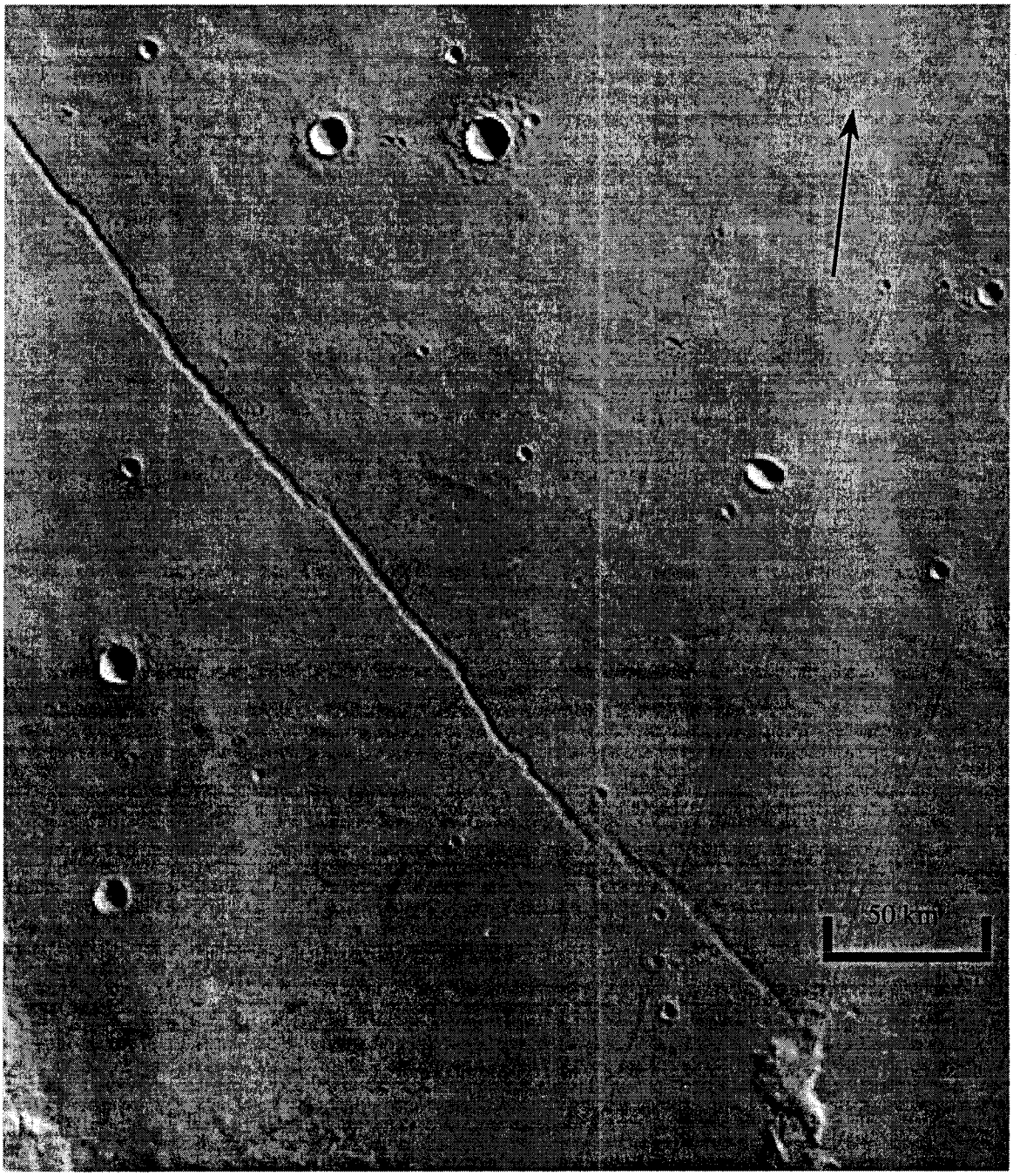

Figure 2b Simple grabens and nearby, similar trending associated pit crater chains in southeastern Noctis Labyrinthus (15S, 97W). (Mars Digital Image Map, MI15S097).

Figure 2c Simple and complex grabens in Claritas Fossae (25S, 107W). Complex grabens are characterized by 10-50 km wide nested grabens that form stepped sides. Notice the large (~100 km wide) north-trending rift formed by the large, shaded down-to-the-west fault scarps along the eastern edge of the image and the shallow sunlite multiple down-to-the-east faults in the center of the image. (Mars Digital Image Map, MI25S107).

Figure 2d Possible tension cracks or joints of the Medusa Fossae Formation (10N, 157W). (Mars Digital Image Map, MI10S157).

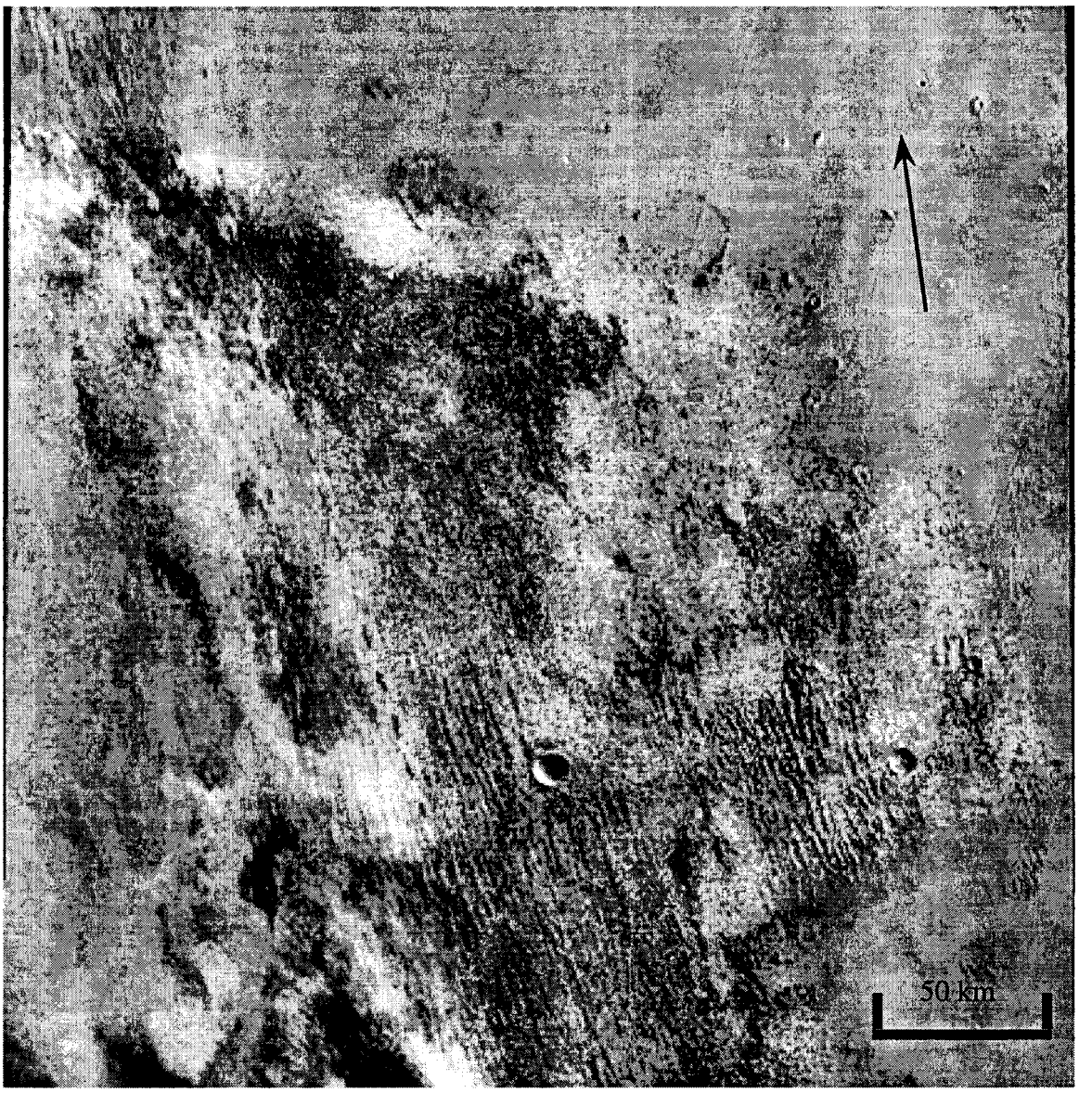

Figure 2e North-northwest trending wrinkle ridges on Lunae Planum (15^{O}N, 67^{O}W). Notice the tension crack on the left central portion of the image. (Mars Digital Image Map, MG15N067).

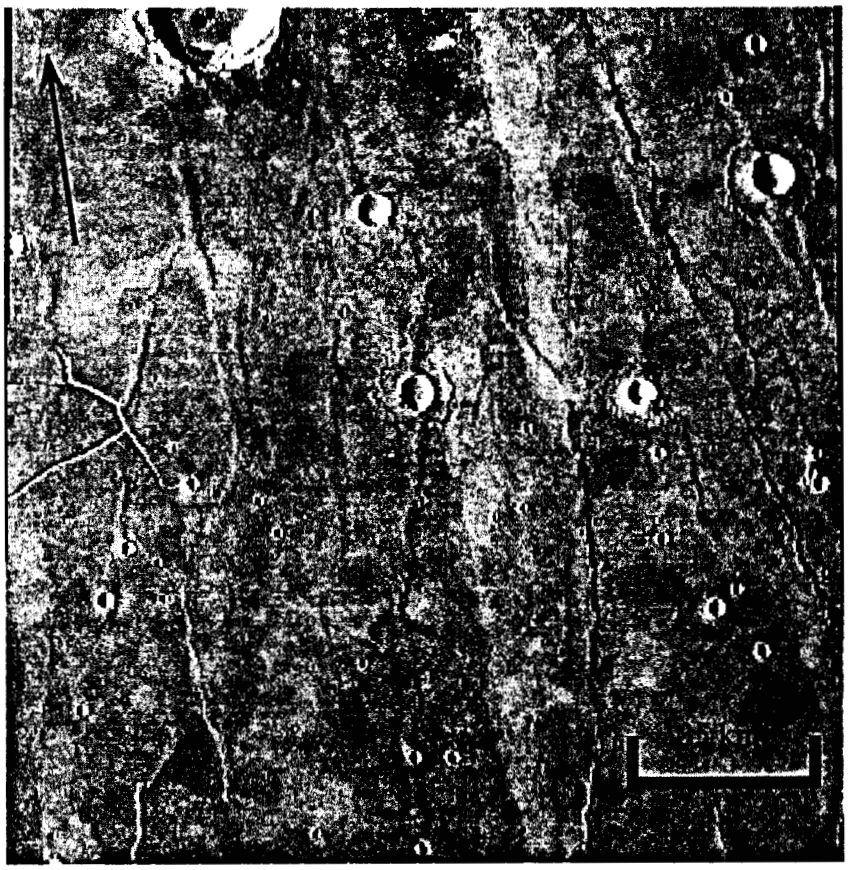

Figure 3a) Number of extensional features identified per stage. b) Number of simple grabens normalized to the total number of mapped features per stage.

A

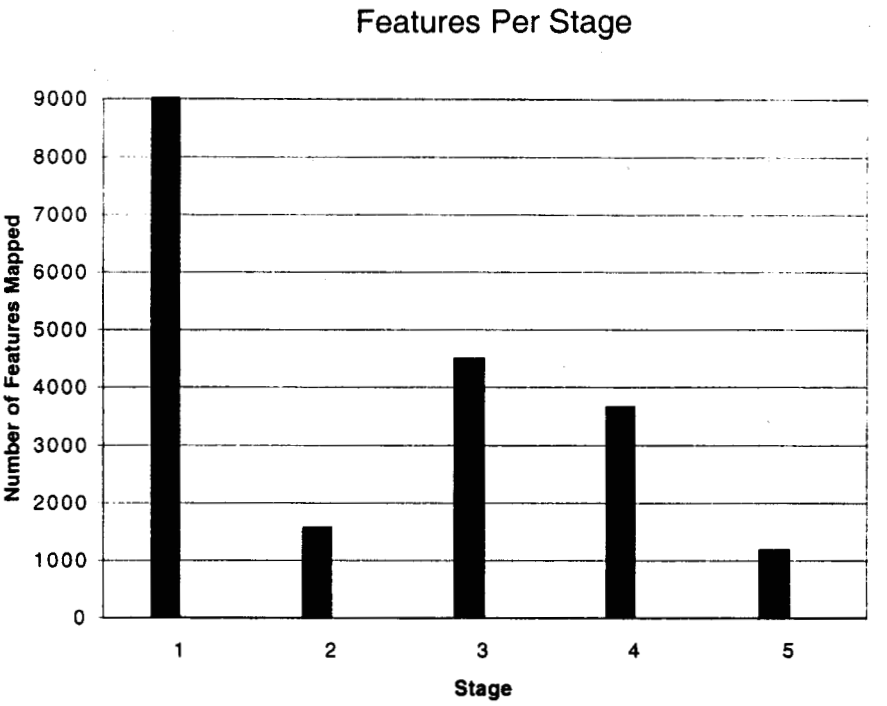

B

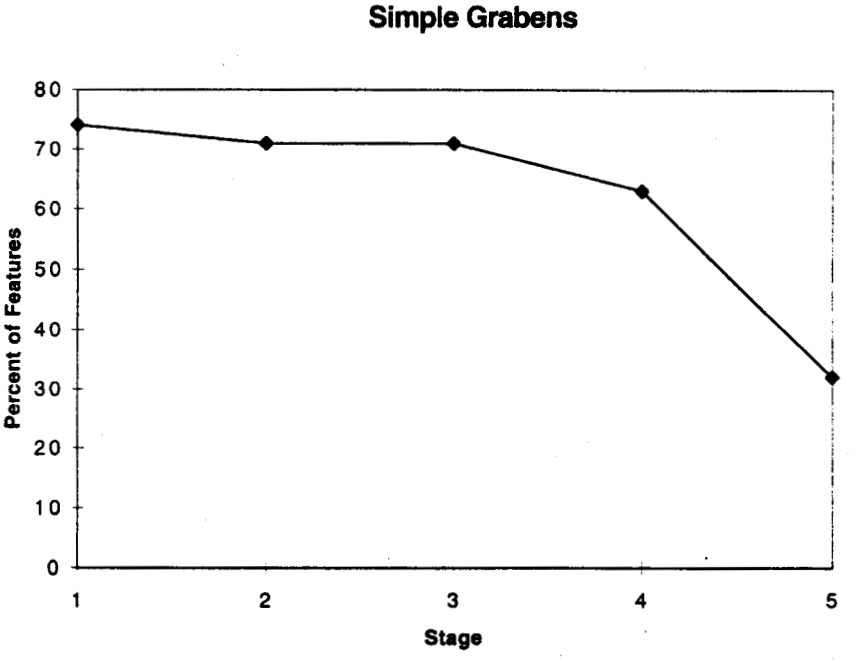

Figure 4 (a) Extensional features mapped for the western hemisphere of Mars from Figure 1. Contour plot of the total number of extensionalfeatures obtained from the vector analysis technique (Contour interval = 200 fault intersections: center = 1,339 radial features or 6.7%). Black shaded areas represent primary centers of tectonic activity; grey shaded areas represent secondary centers listed in Table3 (b) Contour plot of the total number of extensional features from the Beta analysis technique (Contour interval represents density of intersections of 2%.

a.

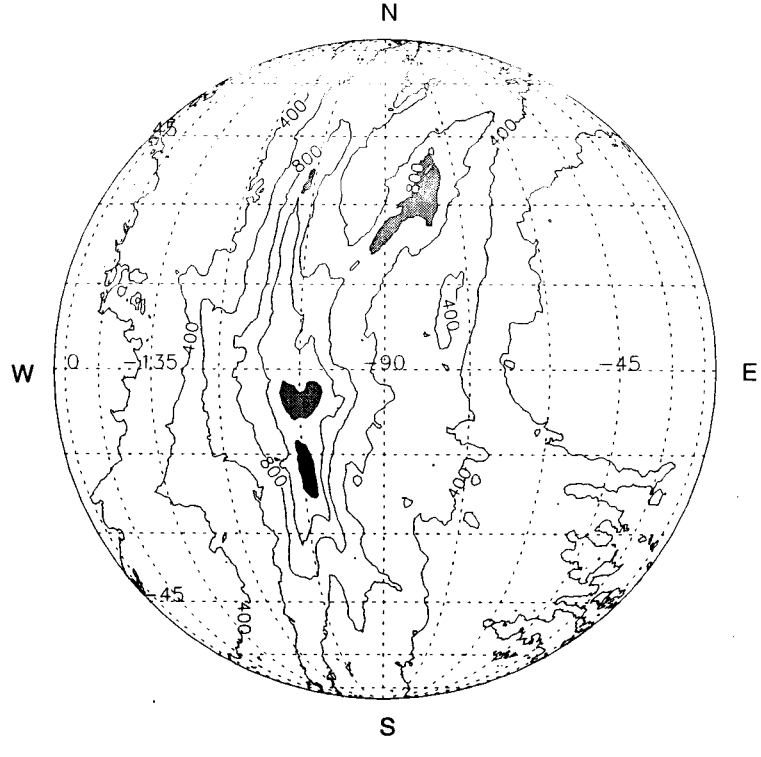

b.

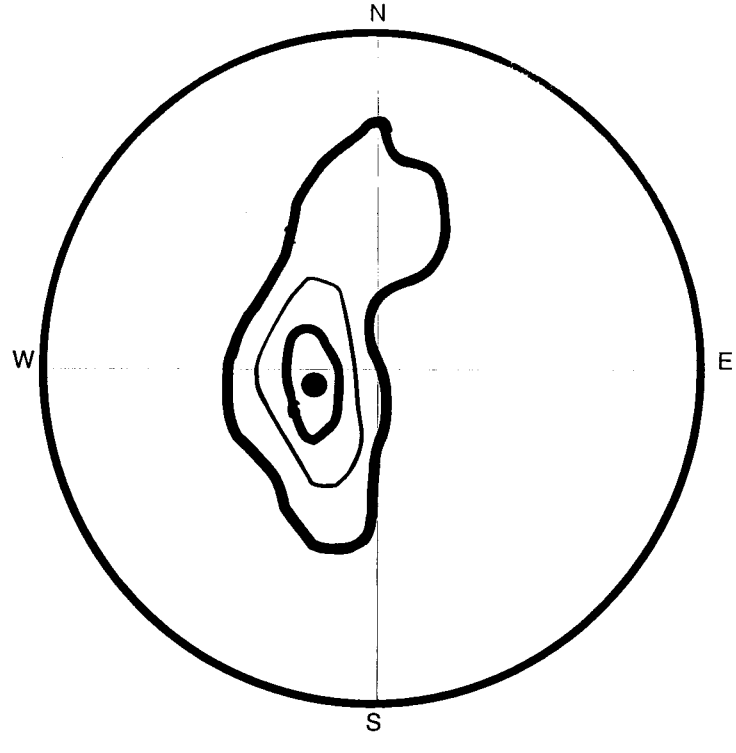

Figure 5 (a) Extensional and compressional features mapped for the western hemisphere of Mars from Figure 1. Contour plot of the total number of features obtained from the vector analysis technique (Contour interval = 250 fault intersections: center = 1,464 radial features or 6%). Black shaded areas represent primary centers of tectonic activity; grey shaded areas represent secondary centers listed in Table 3 (b) Contourplot of the total number of features from the Beta analysis technique (Contour interval represents density of intersections of 2%.

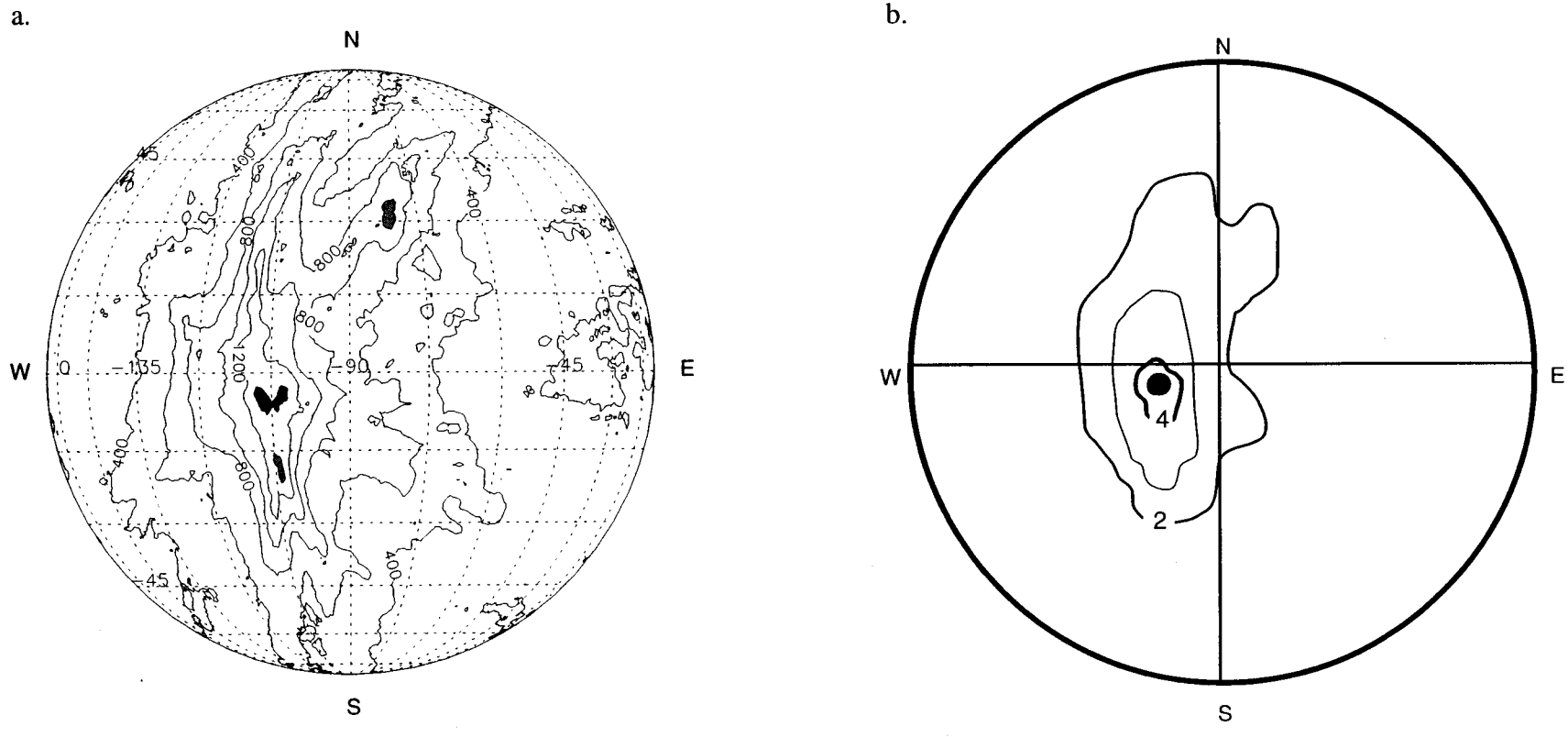

Figure 6 (a) Stage 1 features mapped for the western hemisphere of Mars. (b) Contour plot of Stage 1 features obtained from the vector analysis technique (Contour interval = 125 fault intersections: center = 858 radial features or 9.6%). Black shaded areas represent primary centers of tectonic activity; grey areas represent secondary concentrations. (c) Contour plot of the Stage 1 features from the Beta analysis technique (Contour interval represents density of intersections of 2%.

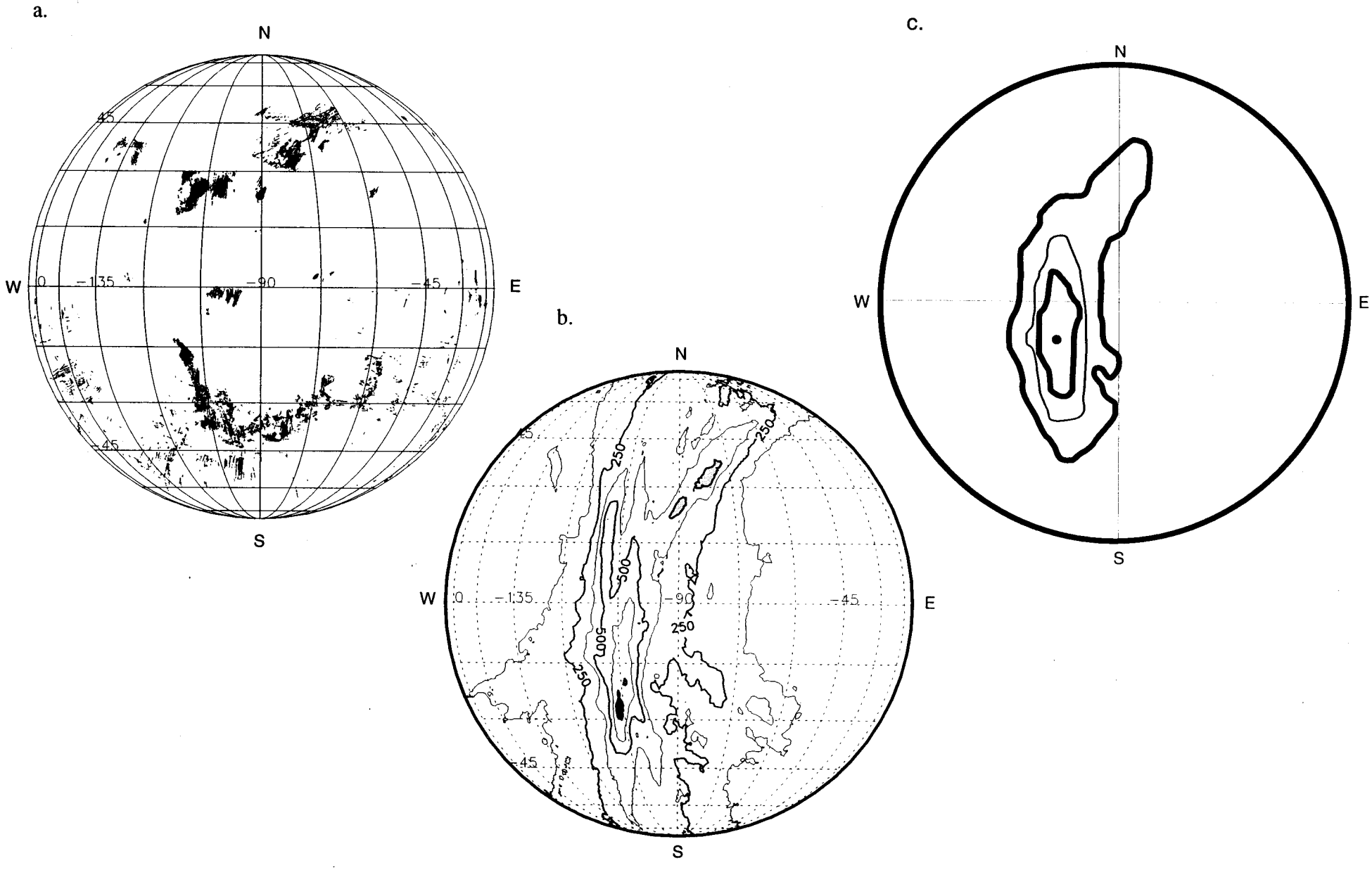

Figure 7 (a) Stage 2 features mapped for the western hemisphere of Mars. (b) Contour plot of Stage 2 features obtained from the vector analysis technique (Contour interval = 50 fault intersections: center = 207 radial features or 13.1%). Black shaded areas represent primary centers of tectonic activity; grey areas represent secondary concentrations. (c) Contour plot of the Stage 2 features from the Beta analysis technique (Contour interval represents density of intersections of 3%).

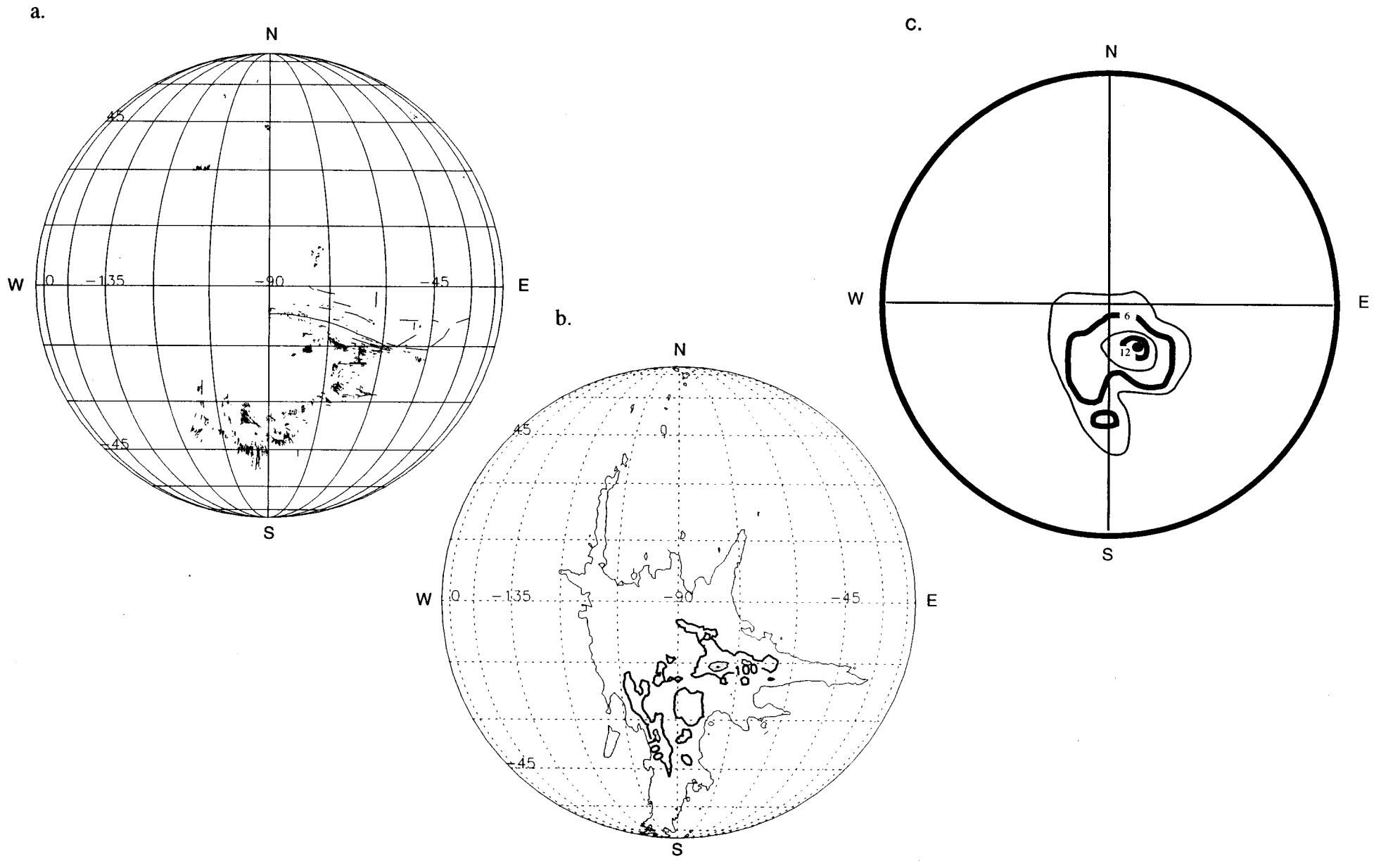

Figure 8 (a) Stage 3 features mapped for the western hemisphere of Mars. (b) Contour plot of Stage 3 features obtained from the vector analysis technique (Contour interval = 100 fault intersections: center = 379 radial features or 8.4%). Black shaded areas represent primary centers of tectonic activity; grey areas represent secondary concentrations. (c) Contour plot of the Stage 1 features from the Beta analysis technique (Contour interval represents density of intersections of 2%).

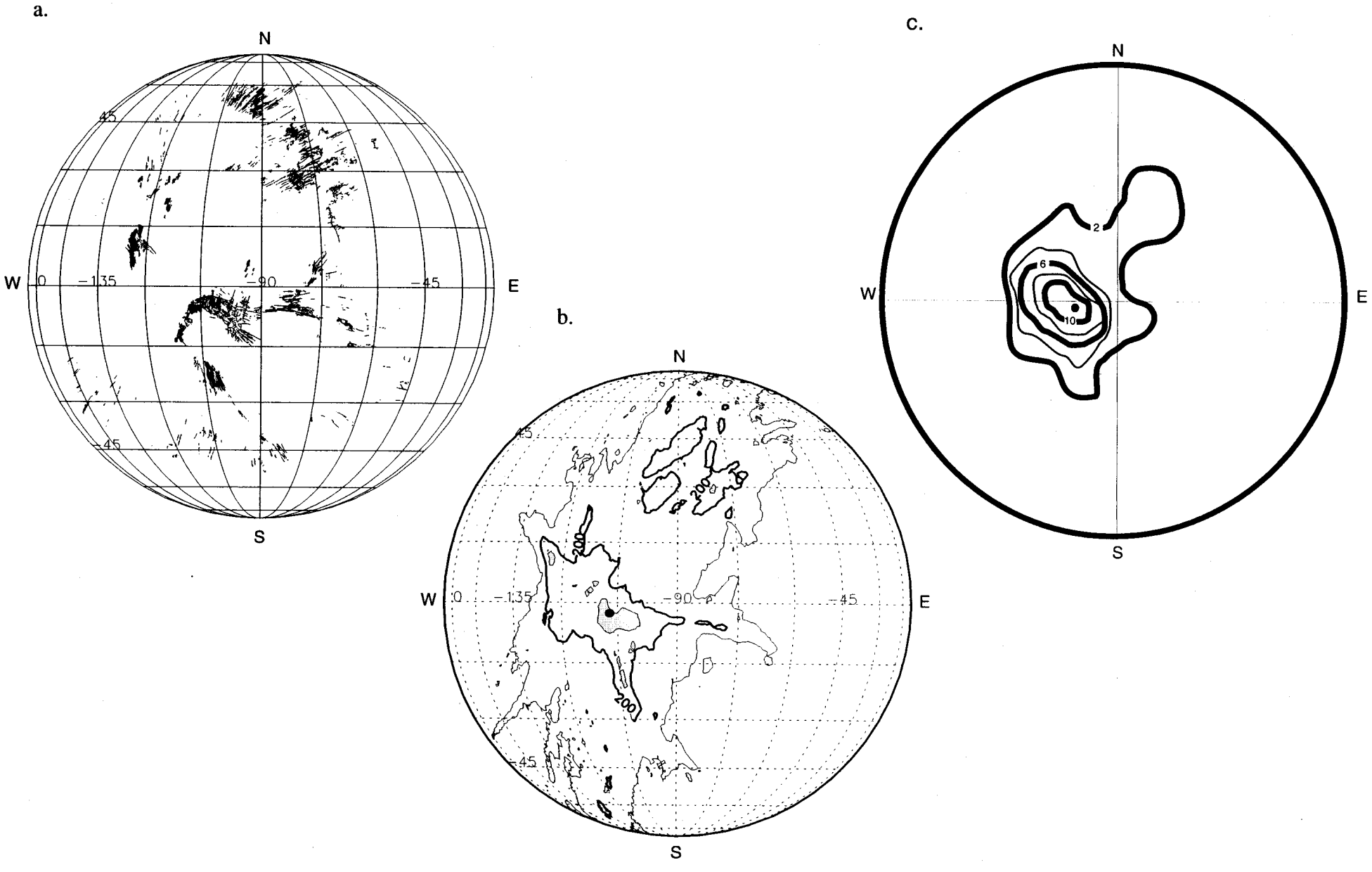

Figure 9 (a) Compressional features mapped for the western hemisphere of Mars. (b) Contour plot of the results obtained from the vector analysis technique for wrinkle ridges. Shaded areas indicate two broad concentrations of features. (Contour Interval = 75 features: center = 394 features or 8.7% of data). (c) Contour plot of wrinkle ridges obtained from the Beta analysis technique (Contour interval represents density of intersections of 1%).

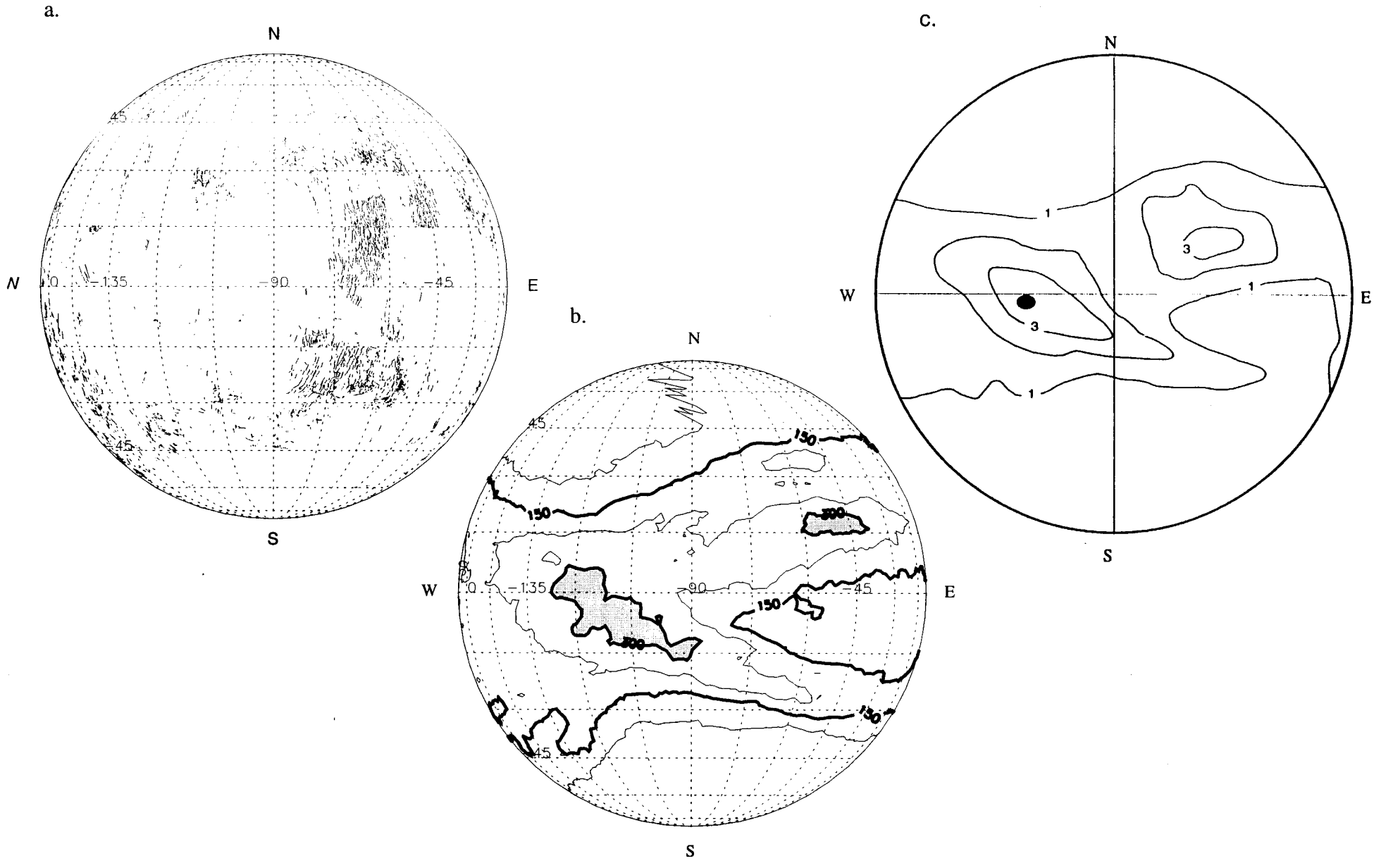

Figure 10 (a) Stage 3 extensional features and ridges mapped for the western hemisphere of Mars. Contour plot of the total number of features obtained from the vector analysis technique (Contour interval = 100 fault intersections: center = 567 radial features or 6%). Grey shaded areas represent primary centers of tectonic activity. (b) Contour plot of the total number of extensional features from the Beta analysis technique (Contour interval represents density of intersections of 2%).

a.

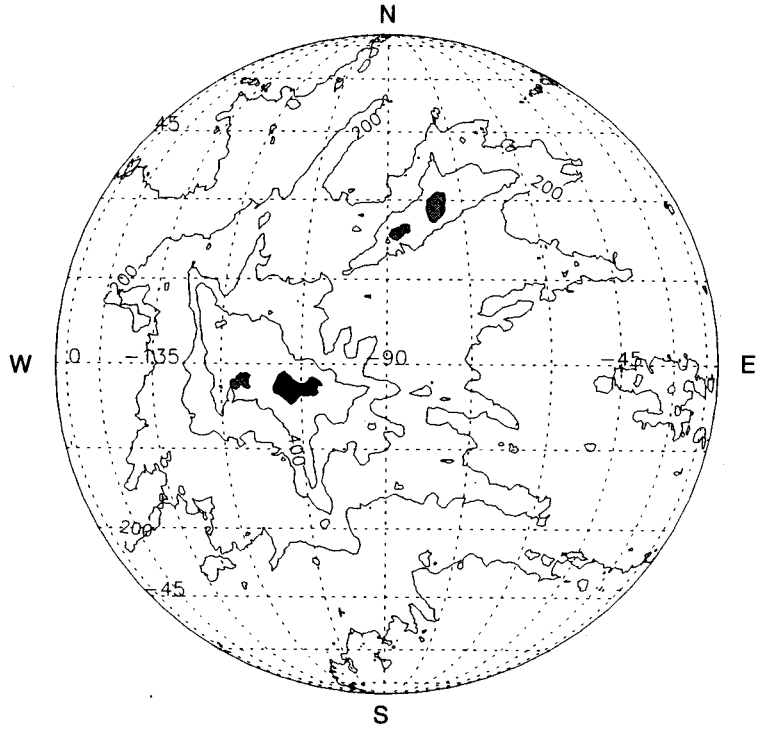

b.

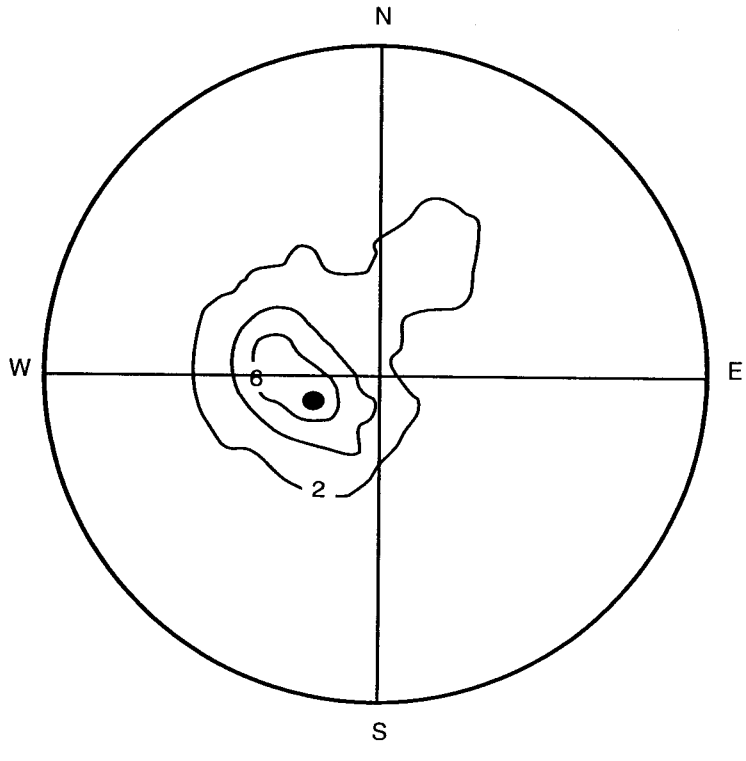

Figure 11 (a) Stage 5 features mapped for the western hemisphere of Mars. (b) Contour plot of Stage 5 features obtained from the vector analysis technique (Contour interval = 50 fault intersections: center = 207 radial features or 17.5%). Black shaded areas represent primary centers of tectonic activity; grey areas represent secondary concentrations. (c) Contour plot of the Stage 5 features from the Beta analysis technique (Contour interval represents density of intersections of 3%).